Polymer Chemistry

Design, Synthesis, and Characterization of Vinyl-addition Polynorbornenes with Tunable Thermal Properties

Journal:	*Polymer Chemistry*
Manuscript ID	PY-ART-08-2021-001050.R1
Article Type:	Paper
Date Submitted by the Author:	17-Sep-2021
Complete List of Authors:	Wang, Xinyi; University of Tennessee, Knoxville, Chemistry Jeong, Yewon; University of Tennessee, Knoxville, Chemical and Biochemical Engineering Love, Christopher; University of Tennessee, Knoxville, Chemistry Stretz, Holly A.; Tenessee Tech University, Chemical Engineering Stein, Gila; University of Tennessee, Long, Brian; University of Tennessee, Knoxville, Chemistry

ARTICLE

Design, Synthesis, and Characterization of Vinyl-addition Polynorbornenes with Tunable Thermal Properties

Received 00th January 20xx,
Accepted 00th January 20xx

DOI: 10.1039/x0xx00000x

Xinyi Wang,[a] Yewon L. Jeong,[b] Christopher Love,[a] Holly Stretz,[c] Gila E. Stein,[b]* Brian K. Long[a]*

Unfunctionalized vinyl-addition polynorbornene (VAPNB) possesses many outstanding properties such as high thermal, chemical, and oxidative stability. These features make VAPNB a promising candidate for many engineering applications. However, VAPNB has a small service window between its glass transition temperature (T_g) and decomposition temperature (T_d), and it cannot be readily processed in a melt state. In this work, we demonstrate that the service window of VAPNBs can be tailored through the use of norbornene monomers bearing alkyl, aryl, and aryl ether substituents. The vinyl addition homopolymerization and copolymerization of these functionalized norbornyl-based monomers yielded VAPNBs with high T_g's (> 150 °C) and large service windows (T_d - T_g > 100 °C), which is comparable to other commercial engineering thermoplastics. To further establish the feasibility of melt processing, a functionalized VAPNB material with T_g = 209 °C and a service window of 170 °C was successfully extruded and molded into bars. Subsequent characterization of the bars by dynamic mechanical analysis (DMA), nuclear magnetic resonance spectroscopy (NMR), and gel permeation chromatography (GPC) revealed only minor signs of polymer degradation. These studies suggest that substituted VAPNBs could be developed into a new class of engineering thermoplastics that is compatible with workhorse melt processing techniques such as extrusion and injection molding, as well as emerging techniques such as extrusion-based 3D printing.

Introduction

Unfunctionalized vinyl-addition polynorbornene (VAPNB) possesses many outstanding properties, such as high thermal, chemical, and oxidative stability,[1] as well as low birefringence,[2] a low dielectric constant,[3, 4] and low moisture absorbance.[5, 6] These properties make VAPNB a promising candidate for many engineering and high-performance applications. However, unfunctionalized VAPNB has limited solubility in organic solvents,[7, 8] mechanical brittleness,[9] and a small service window between its glass transition (T_g) and decomposition temperatures (T_d),[7] all of which limit its processability.[9] Several studies have shown that the homopolymerization and/or copolymerization of norbornyl monomers bearing polar or nonpolar substituents can improve both polymer solubility and mechanical properties.[3, 10-14] Such functionalized VAPNBs can often be solution processed into mechanically robust, freestanding films that are suitable for a variety of potential applications, including gas separations,[1, 10, 13, 15] pervaporation membranes,[11] ion-exchange membranes,[16, 17] high-frequency interconnects,[12] and nonlinear-optical devices.[2] In contrast, in the fields of extrusion, injection molding, film blowing, or 3D printing, where commercial thermoplastics[18-23] are widely used, few comprehensive studies of improving VAPNB melt processability by employing substituted norbornene monomers exist in the peer-reviewed literature.[14, 24]

To facilitate the melt processing of VAPNBs, their glass transition temperature (T_g) must be lowered while maintaining a high decomposition temperature (T_d) to establish a broad service window and enable melt flow without decomposition. Indeed, prior reports have demonstrated that certain functionalized VAPNBs may exhibit depressed T_g's while simultaneously maintaining high T_d's,[10, 12-14, 16, 17, 25] and companies such as BFGoodrich and Promerus have commercialized several VAPNB derivatives with T_gs well below that of unsubstituted VAPNB.[2, 3, 6, 26-29] As an example, Goodall and coworkers showed that copolymerization of alkyl-substituted norbornenes and unsubstituted norbornene could be used to fine-tune VAPNB T_g,[25] suggesting that melt processable VAPNBs may be accessed through careful substituent choice. This was also demonstrated by another recent report by Kim, Park, Huh and coworkers.[14] However, the overall relationships between thermal properties and molecular design are difficult to infer from current literature due to broad variability in the synthetic and thermal characterization methods used.[4, 7, 8, 11, 15, 30, 31] For example, polymer microstructure (i.e. stereoregularity, tacticity) may be strongly influenced by the type of catalyst used, and these attributes may impact resultant thermal properties.[1, 2, 32] Additional complications arise in that commonly employed techniques for characterization of T_g, such as differential scanning calorimetry (DSC),[8] spectroscopic ellipsometry,[33] and dynamic mechanical

[a] Department of Chemistry, University of Tennessee, Knoxville, Tennessee, 37996-1660, United States.
[b] Department of Chemical & Biomolecular Engineering, University of Tennessee, Knoxville, Tennessee, 37996-1660, United States.
[c] Department of Chemical Engineering, Tennessee Tech University, Cookeville, Tennessee, 38505, United States
Electronic Supplementary Information (ESI) available: [details of any supplementary information available should be included here]. See DOI: 10.1039/x0xx00000x

analysis (DMA),[12, 13, 15] often produce values that do not agree well with one another, particularly as each method probes a different property.

To provide fundamental insight into how monomer substituent structure may be used to tailor VAPNB T_g and service window (T_d - T_g), we examined a systematic series of substituted VAPNB homopolymers and copolymers bearing polar and/or nonpolar functional groups. To ensure consistency and comparability of results, all polymers were synthesized using a single catalyst/activator system[34] under identical reaction conditions. The T_d of each polymer was measured by thermogravimetric analysis (TGA), and T_g was measured using DMA. For a few selected polymers, these T_g values were then compared to those measured using DSC and spectroscopic ellipsometry. Copolymer T_g values were compared to predictions based on homopolymer values using either the Fox or Gordon-Taylor equations, providing insight into the predictive capability of these simple correlations when substituents differing in structure and intermolecular interactions (e.g., London dispersion forces, π-π stacking, and dipole-dipole interactions) are introduced.

Though melt processing of VA-PNBs remains virtually unexplored in the peer-reviewed literature, recent work by Kim, Park, Huh and coworkers used melt pressing to prepare thin samples of unsubstituted-co-alkyl-substituted VAPNBs for tensile testing.[14] However, to the best of our knowledge, there are no literature examples in which melt extrudability is demonstrated. While a broad service window is required for thermal processing, this condition is not sufficient to establish processability by techniques such as melt extrusion. Therefore, to conclude our study, we selected a substituted VAPNB with a broad service window (T_d - T_g ≈ 200 °C) for extrusion tests. We found that this substituted VAPNB exhibited melt processability similar to that of polystyrene (**PS**), and characterization of the extruded material by GPC, NMR spectroscopy, and DMA showed negligible signs of polymer degradation. These studies demonstrate that substituted VAPNBs may be engineered to enable their processing by workhorse techniques such as extrusion, thereby potentially broadening the application scope of this class of high-performing polyolefin-based materials.

Experimental Section

General Materials and Methods. All reactions were conducted under an inert atmosphere using an MBraun glovebox and a dry nitrogen atmosphere, unless noted otherwise. Synthesized monomers were purified via sequential distillations (≥ 98% purity, via GC) unless otherwise noted, degassed via freeze–pump–thaw (×3), and stored over 3 Å molecular sieves in a glovebox prior to use. Dicyclopentadiene, hydroquinone, 1-hexene, 1-octene, and sodium borohydride were purchased from Acros Organics and used as received. 1-Decene and 1-dodecene were purchased from TCI America and used as received. 5-Norbornene-2-carboxaldehyde and benzyl bromide were purchased from Alfa Aesar and used as received. Sodium hydride, allylmagnesium chloride solution (2.0 M in THF), and (2-bromoethyl)benzene were purchased from Sigma-Aldrich and used as received. Hexane, ethyl acetate, methanol, and chloroform were purchased from Fisher Scientific and used as received. Dichloromethane for polymerizations was purchased from Fisher Scientific and purified using an Innovative Technologies PureSolv Solvent Purification System and degassed via freeze-pump-thaw (×3) prior to use. The catalyst (η^3-allyl)Pd(i-Pr$_3$P)Cl was synthesized according to literature procedure and stored in a glovebox prior to use.[34] This catalyst is commonly used for vinyl-addition polymerization of norbornene-based monomers.[11, 15, 17, 31] Lithium tetrakis(pentafluorophenyl)borate ethyl etherate (LiBAr$^F_4$) was obtained as a gift from Boulder Scientific and used as received. Monomers **M1**-**M4** were synthesized according to prior literature reports with only minor modifications.[35, 36] The intermediate 5-phenyl-1-pentene,[37] 5-norbornene-2-methanol[38] and 5-benzyloxymethyl-2-norbornene (**M6**)[38-40] were synthesized according to prior literature reports and all characterization matched those previously reported. **PS** (M_w ~ 350 kg/mol, M_n ~ 170 kg/mol) was purchased from Sigma Aldrich and used as a comparison sample for thermal characterization, melt processing, and mechanical characterization.

Synthesis of 5-butyl-2-norbornene (M1). Monomer **M1** was synthesized following a modified literature procedure.[35, 36] 1-Hexene (4.0 g, 47.5 mmol), dicyclopentadiene (2.5 g, 18.9 mmol), and hydroquinone were added to a 50 mL glass pressure tube with a stir bar. The pressure tube was sealed and heated to 240 °C for 3 h with stirring. After cooling, the mixture was purified by two sequential distillations at reduced pressure (10 torr, 88-90 °C) to yield 0.58 g of monomer **M1** (10.3% yield) as a mixture of *endo*:*exo* isomers (*endo*:*exo* = 75:25). All characterizations matched prior literature reports.[35]

Synthesis of 5-hexyl-2-norbornene (M2). Monomer **M2** was synthesized following the procedure described for **M1.** The crude mixture of **M2** was purified by two sequential distillations at reduced pressure (4 torr, 113-115 °C) to yield 1.11 g of monomer **M2** (16.5% yield) as a mixture of *endo*:*exo* isomers (*endo*:*exo* = 79:21). All characterizations matched prior literature reports.[41]

Synthesis of 5-octyl-2-norbornene (M3). Monomer **M3** was synthesized following the procedure described for **M1.** The crude mixture of **M3** was purified by two sequential distillations at reduced pressure (4 torr, 132-134 °C) to yield 1.11 g of monomer **M3** (17.0% yield) as a mixture of *endo*:*exo* isomers (*endo*:*exo* = 79:21). ^{1}H NMR ($CDCl_3$, 293 K, *endo* isomer): δ (ppm) = 6.10 (1H, dd), 5.91 (1H, dd), 2.75 (2H, m), 1.96 (1H, m), 1.83 (1H, m), 1.39 (1H, m), 1.35-1.22 (12H, m), 1.19 (1H, m), 1.07 (2H, m), 0.88 (3H, t), 0.48 (1H, ddd). ^{13}C NMR ($CDCl_3$, 293 K, endo/exo mixture): δ (ppm) = 137.16, 137.03, 136.36, 132.67, 49.78, 46.59, 45.64, 45.44, 42.75, 42.09, 39.00, 36.87, 35.06, 33.33, 32.68, 32.17, 30.19, 30.17, 29.92, 29.90, 29.59, 29.13, 28.91, 22.93, 14.35. HRMS^{calc} $C_{15}H_{26}$ (H^+ adduct) = 207.2113 m/z. HRMS^{expt} $C_{15}H_{26}$ (H^+ adduct) = 207.1858 m/z.

Synthesis of 5-decyl-2-norbornene (M4). Monomer **M4** was synthesized following the procedure described for **M1.** The crude mixture of **M4** was purified by two sequential distillations at reduced pressure (0.5 torr, 110-112 °C) to yield 1.11 g of

monomer **M4** (12.1% yield) as a mixture of *endo*:*exo* isomers (*endo*:*exo* = 78:22). ^{1}H NMR ($CDCl_3$, 293 K, *endo* isomer): δ (ppm) = 6.10 (1H, dd), 5.91 (1H, dd), 2.75 (2H, m), 1.96 (1H, m), 1.83 (1H, m), 1.39 (1H, m), 1.35-1.22 (16H, m), 1.19 (1H, m), 1.07 (2H, m), 0.88 (3H, t), 0.48 (1H, ddd). ^{13}C NMR ($CDCl_3$, 293 K, endo/exo mixture): δ (ppm) = 137.16, 137.03, 136.36, 132.67, 49.78, 46.59, 45.64, 45.44, 42.75, 42.09, 39.00, 36.87, 35.07, 33.33, 32.68, 32.17, 30.19, 30.17, 29.96, 29.94, 29.90, 29.60, 29.14, 28.91, 22.93, 14.35. HRMS^{calc} $C_{17}H_{30}$ (H^+ adduct) = 235.2426 m/z. HRMS^{expt} $C_{17}H_{30}$ (H^+ adduct) = 235.2161 m/z.

Synthesis of 5-phenylpropyl-2-norbornene (M5). The reagent 5-phenyl-1-pentene was synthesized following a known literature procedure.[37] 5-phenyl-1-pentene (5.84 g, 39.9 mmol), dicyclopentadiene (2.14 g, 16.2 mmol), and hydroquinone were added to a 50 mL glass pressure tube with a stir bar. The pressure tube was then sealed and heated to 240 °C for 12 h with stirring. The mixture was cooled to room temperature and purified by two sequential distillations at reduced pressure (0.5 torr, 130-132 °C) to yield 1.75 g of monomer **M5** (25.4% yield) as a mixture of *endo*:*exo* isomers (*endo*:*exo* = 76:24). ^{1}H NMR ($CDCl_3$, 293 K, *endo* isomer): δ (ppm) = 7.31-7.17 (5H, m), 6.11 (1H, dd), 5.90 (1H, dd), 2.77 (2H, m), 2.58 (2H, m), 2.01 (1H, m), 1.84 (1H, m), 1.74-1.08 (6H, m), 0.50 (1H, ddd). ^{13}C NMR ($CDCl_3$, 293 K, endo/exo mixture): δ (ppm) = 143.12, 143.03, 137.16, 137.08, 136.40, 132.55,128.55, 128.45, 128.42,125.79, 125.76, 49.77, 46.56, 45.58, 45.45, 42.73, 42.09, 38.91, 38.86, 36.47, 36.43, 34.72, 33.26, 32.61, 30.98, 30.79. HRMS^{calc} $C_{16}H_{20}$ (H^+ adduct) = 213.1643 m/z. HRMS^{expt} $C_{16}H_{20}$ (H^+ adduct) = 213.1407 m/z.

General polymerization procedure. Under air-free conditions (glovebox), (η^3-allyl)Pd(i-Pr$_3$P)Cl (10 μmol), LiBAr$^F_4$ (10 μmol), and dry/degassed DCM (1 mL) were combined in a 20 mL scintillation vial and stirred for 20 min to activate the catalyst. In a separate vial, the monomer (or monomers) (5 mmol, total) was dissolved in dry/degassed DCM (4 mL) and added to the stirred catalyst solution. All polymerizations were ran overnight, unless otherwise noted, before quenching via exposure to air, dilution with additional DCM (10 mL), and precipitation into 250 mL of methanol. All polymers were isolated by vacuum filtration and dried in *vacuo* until reaching constant weight.

Monomer and Polymer Characterization. ^{1}H and ^{13}C NMR spectra of monomers and polymers were obtained in $CDCl_3$ using a Varian 300 MHz or Varian 500 MHz NMR instrument, and spectra were referenced to the residual solvent peak at δ = 7.26 ppm (^{1}H) and 77.23 ppm (^{13}C), respectively. High-resolution mass spectrometry (HRMS) was performed using a JEOL AccuTOF equipped with a DART source. Molecular weight and dispersity (*Đ*) of all polymers were determined using a Tosoh EcoSEC GPC with a refractive index detector and THF as the eluent at 40 °C. All MW's and dispersity values are reported relative to polystyrene standards.

Thermal Characterization of Polymers. Thermogravimetric analysis (TGA) was performed using a TA Instruments Q550 with a heating rate of 10 °C/min under a N_2 purge. All T_d values are reported as the temperature corresponding to 5% weight loss. To measure T_g, three methods were employed: modulated DSC (MDSC), spectroscopic ellipsometry, and DMA. MDSC measurements were performed using compressed polymer powders in T-zero pans with a TA Instruments Q2000 at a heating rate of 3 °C/minute (modulated at ± 1.00 °C per 60 s) from 80 to 300 °C under a nitrogen atmosphere. T_g was determined based upon the transition of reversing heat capacity. DMA was performed using a TA Instruments RSA-G2 solids analyzer equipped with a tension fixture. Thick VAPNB film samples (40-120 μm) were prepared by solution casting from $CHCl_3$ solutions (3 wt%) into a PTFE dish. For example, a desired polymer (0.5 g) was added to $CHCl_3$ (10 mL) and stirred until fully dissolved. The solution was filtered through a 0.45 μm PTFE syringe filter into a clean and leveled PTFE dish that is approximately 6 cm in diameter. In contrast, polystyrene films were prepared by dissolving the commercial polystyrene sample (0.5 g) in toluene (3 mL), which was then filtered through a 0.45 μm PTFE syringe filter, degassed, and poured onto a levelled glass plate and drawn using a blade coater under a controlled shear rate. The solution cast VAPNB and drawn polystyrene films were covered to reduce the rate of evaporation while drying, and the polymer films were collected after complete solvent evaporation. Resultant films were determined to be 40-120 μm in thickness and were cut into strips (3-5 mm wide by 10-15 mm long) for DMA testing. The strips were mounted in the tension fixture, equilibrated at the starting temperature for 5 min, and the experiment was run at a heating rate of 5 °C/min from either 100 °C or 40 °C up to 300 °C under a nitrogen atmosphere with an axial force oscillated at 0.1% strain rate and 1 Hz. The T_g was taken as the maximum of the tan δ curve, and the reported value is the average of two measurements. Spectroscopic ellipsometry was used to measure thin film T_g's. Films were prepared by spin casting from a toluene solution (~5 wt%) onto a silicon wafer and heated to 240 °C for 20 min under a nitrogen atmosphere to drive-off residual solvent. All films were 500 ± 50 nm in thickness. A J.A. Woollam M-2000 spectroscopic ellipsometer (wavelengths λ = 300 – 1690 nm) was used to record the ellipsometry parameters Δ and ψ as a function of temperature. The incidence/detection angles were fixed at 70˚, and samples were heated/cooled at a rate of 1 °C/min from 80 to 240 °C under a nitrogen atmosphere. The ellipsometry parameters were modeled using a three-layer system of polymer, native oxide, and silicon (in air). The refractive index of the polymer layer was described by the Cauchy dispersion relation, $n(\lambda) = A + B/\lambda^2$, and the refractive index of both native oxide and silicon were fixed to known literature values. The Cauchy constants (*A* and *B*) and polymer film thickness *h* were adjustable parameters for regression analysis. Typical values for *A* and *B* parameters were around 1.5 and 0.005-0.008, respectively. The T_g was determined as the point of change in slope on a plot of polymer film thickness versus temperature[42] using data from the second cooling cycle. The T_g is taken as the intersection of the two lines that capture the rubber and glass regimes, as shown in Figures S46-S51 in the Supporting Information.

Melt Extrusion and Characterization of Mechanical Properties. All polymer samples were dried *in vacuo* at 85 °C

overnight prior to use. Tensile bars were prepared using a DSM Micro-5 twin screw compounder and benchtop injection molding machine, which was operated at a barrel temperature of 210 °C for commercial polystyrene samples and 250 °C for VAPNBs, a mold temperature of 100 °C under N_2 purge, 90 rpm, a melt index of 10-12 g/10 min, and a back force of ~1000-1500 N on the screws. As limited quantities of the synthesized VAPNB materials were available, relative to what was needed for melt processing, these process conditions were deemed best, but were not optimized. A portion of the synthesized VAPNB material was used for purging the extruder to ensure clean extrusion conditions, and bars were checked for clarity by visual inspection using a light box, indicating completeness of purge throughout the process. Mechanical testing was performed using an Instron load frame model 5948 (horizontal testing, 1 kN load cell) at a strain rate of 0.1 mm/min according to ASTM D638. The modulus was obtained by plotting engineering/true stress verses corresponding strain. Cyclic loading moduli were obtained by testing two specimens, each with three cycles of load and unload between 110-360 N.

Wide Angle X-Ray Scattering. Select films (**P3**, **P4**) were illuminated at normal incidence (transmission through the film thickness) under ambient conditions using A Xenocs GeniX 3D microfocus source with a copper target (wavelength λ = 0.154 nm). The sample to detector distance was 0.045 m. A Pilatus3 R_300K detector (Dectris) was used with pixel size of 172 µm × 172 µm. The data acquisition time was 5 min. The two-dimensional images from each measurement were azimuthally-integrated to yield a one-dimensional scattering profile of intensity I(a.u.) versus scattering vector q(Å $^{-1}$).

Discussion

As a basis for the design of melt processable VAPNBs, we surveyed the thermal characteristics of commercially available engineering thermoplastics, such as polysulfone, polyetherimide, and polycarbonate. This analysis revealed that each material displayed a T_g > 150 °C and a T_d - T_g > 100°C.[18-22] In an effort to design VAPNBs that provide a similarly large service window, albeit while maintaining a high T_d, a variety of homopolymers and copolymers were synthesized using substituted norbornene monomers. Monomers **M1**-**M4** (Figure 1) bear linear alkyl substituents of varying length, whereas monomers **M5** and **M6** incorporate bulky aromatic groups that are tethered by an alkyl or ether linkage, respectively. In addition to differences in flexibility and size, these substituents introduce the possibility of different types of intermolecular forces being present. For example, monomers **M1**-**M4** are believed to interact primarily via weak London-Dispersion forces, whereas monomers **M5** and **M6** introduce a bulky benzyl substituent that may participate in π-π stacking interactions that have been reported to improve film formation.[12] Furthermore, monomer **M6** also adds the potential to introduce dipole-dipole interactions as a result of its ethereal moieties.

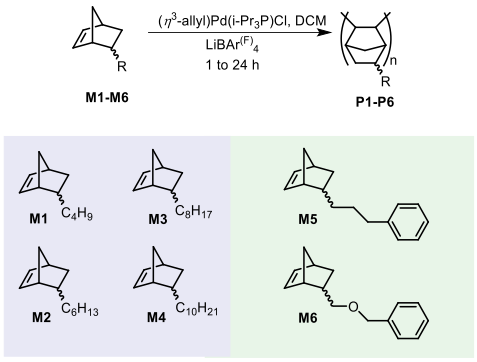

Figure 1. Series of VAPNBs (**P1**-**P6**) chosen to probe the effects of substituent architecture on resultant thermal properties.

Monomers **M1**-**M5** were synthesized via Diels-Alder reaction of *in-situ* cracked dicyclopentadiene and a corresponding dieneophile that was either commercially available or was synthesized following established literature procedures.[37] Each monomer was isolated as a clear liquid following successive vacuum distillations at reduced pressure (10-25% yield) until reaching >98% purity, as determined via gas chromatography. As a note, monomer **M3** could only be obtained in 85% purity due to the presence of impurities having similar boiling points that could not be readily removed via distillation or flash column chromatography. Monomer **M6** was synthesized via Williamson ether synthesis in which 5-norbornene-2-methanol was reacted with benzyl bromide, followed by column chromatography to obtain a clear liquid (61% yield). Each monomer was characterized using ^{1}H NMR spectroscopy to confirm functionalization and determine the *endo*:*exo* ratio of the norbornene substituent.

It is well known that the catalyst employed to access VAPNBs may influence the thermomechanical properties of the resultant materials, an effect that has been attributed to differences in polymer tacticity and stereoregularity.[25, 43, 44] We also observed this in our preliminary studies, wherein both Ni- and Pd-based catalysts were used (see Supporting Information S47, S53-54, S65-67). However, to avoid complications arising from tacticity and stereoregularity differences based upon catalyst choice, we chose to use the catalyst system (η^3-allyl)Pd(i-Pr_3P)Cl/LiBAr$^F_4$ (BAr$^F_4$ = tetrakis(pentafluorophenyl)-borate) for all polymer syntheses described herein. As shown in Scheme 1, monomers **M1**-**M6** were each homopolymerized to yield polymers **P1**-**P6**. In order to further investigate the influence of various substituents on the thermal properties of VAPNBs, a series of statistical copolymers denoted using the notation **PXPY** were synthesized, wherein X and Y signify the two monomer components copolymerized. Specifically, X was fixed as **M2** and Y was either **M4**, **M5**, or **M6** to yield copolymers **P2P4**, **P2P5**, and **P2P6**, respectively.

Each polymer was obtained in modest to excellent yield (62-98%) and was characterized via ^{1}H NMR spectroscopy and gel permeation chromatography (GPC). All polymer molecular weights (M_n) exceeded 60 kg/mol and dispersities ($Đ$) ranged from 1.3-2.8 (Table 1). It was noted that the homopolymerization of **M3** resulted in higher molecular weight, higher dispersity and poorer solubility as compared to other

VAPNB analogues. We hypothesize that this is due to the presence of impurities, such as tricyclopentadiene, that may have been incorporated into the polymer chain and could potentially lead to undesired crosslinking. Thus, a shorter reaction time (1 h) was applied to minimize the potential for crosslinking (Table 1, entry 3). In contrast, the homopolymerization of **M6** (Table 1, entry 6) led to decreased polymer yield and molecular weight, even when polymerized at a higher monomer:catalyst ratio ([mon]:[cat] = 1000:1) and extended reaction time (24 h). Similar observations have been reported in the literature, in which slower polymerization rates and lower yields are often hypothesized to result from deleterious interactions between the polar substituent and the electrophilic, active catalyst species.[9, 11, 43, 45] Similar trends were also found for all copolymerizations (Table 1, entries 13-15).

Table 1. Homo- and co-polymerization of substituted norbornene monomers.[a]

entry	polymer	feed ratio (**MX**:**MY**)	actual ratio[d] (**MX**:**MY**)	yield (%)	M_n[f] (kg/mol)	$Đ$[f]
1	**P1**	100:0	100:0	83	63	1.30
2	**P2**	100:0	100:0	85	84	1.35
3[b]	**P3**	100:0	100:0	64	163	2.81
4	**P4**	100:0	100:0	92	129	2.00
5	**P5**	100:0	100:0	76	89	1.41
6[c]	**P6**	100:0	100:0	62	66	1.32
7	**P2^{75}P4^{25}**	75:25	-[e]	76	166	2.32
8	**P2^{50}P4^{50}**	50:50	-[e]	97	159	2.20
9	**P2^{25}P4^{75}**	25:75	-[e]	94	165	1.91
10	**P2^{68}P5^{32}**	75:25	68:32	96	92	1.47
11	**P2^{44}P5^{56}**	50:50	44:56	98	94	1.42
12	**P2^{15}P5^{85}**	25:75	15:85	97	94	1.46
13[c]	**P2^{86}P6^{14}**	75:25	86:14	83	126	1.28
14[c]	**P2^{65}P6^{35}**	50:50	65:35	75	102	1.29
15[c]	**P2^{28}P6^{72}**	25:75	28:72	78	96	1.32

[a]General polymerization conditions: total monomer concentration = 5 mmol, [catalyst] = 10 µmol, 5 mL of DCM, room temperature, and t_{rxn} = 16 h. [b]Reaction time (t_{rxn}) = 1 h. [c][mon]:[cat] = 1000:1 and t_{rxn} = 24 h. [d]Monomer incorporation ratios (**MX:MY**) were calculated via ^{1}H NMR spectroscopy. [e]The monomer incorporation ratio (**MX:MY**) could not be determined via ^{1}H NMR spectroscopy due to overlapping ^{1}H resonances. [f]Molecular weights and dispersities were measured using gel permeation chromatography at 40 °C in THF and are reported relative to polystyrene standards.

Copolymer compositions are denoted as **PX^{n}PY^m**, where the superscripts "n" and "m" represent the actual monomer incorporation ratios of each monomer (**MX**:**MY**). Monomer incorporation ratios for the **P2P4** copolymer series (entries 7-9) could not be determined by ^{1}H NMR spectroscopy due to the significant overlap of all peaks in the alkyl region; however, the incorporation ratios for the copolymer series **P2P5** and **P2P6** (Table 1, entries 10-15) were readily determined based upon integration of their benzylic proton resonances corresponding to monomers **M5** (2.59 ppm) and **M6** (4.49 ppm), respectively, to all remaining protons in alkyl region. Therein, we found that copolymerizations of **M2** and **M5** favored higher incorporations of **M5** than included in the feed, whereas copolymerizations of **M2** and **M6** favored higher incorporation of **M2** than predicted based upon the monomer feed ratio. The lower observed incorporations of monomer **M6** is consistent with the reduced polymerization rate often observed for monomers bearing polar substituents.[46]

As previously mentioned, VAPNB T_g values can be probed via several techniques, such as DSC, DMA, and ellipsometry.[8, 12, 13, 15, 33] Unfortunately, each of these methods determines T_g by probing a different polymer property, resulting in data that may not be directly comparable to results obtained via another method. For example, DSC detects T_g through changes in heat capacity above and below the glass transition, whereas DMA probes changes in viscoelastic properties (and depends on whether T_g was determined based upon storage modulus (E'), loss modulus (E''), or tan δ peak), and ellipsometry detects T_g through changes in the linear coefficient of thermal expansion.[47] We chose to evaluate all three techniques using a subset of the polymers described in Table 1 so as to compare each method of T_g determination. The polymers selected for this comparison were homopolymers **P2**, **P6**, the **P2P6** copolymer series, and a **PS** control. Lastly, because the T_g of each substituted VAPNB could not be detected using conventional DSC, MDSC was used for all studies described herein.[48]

As shown in Table 2, the T_g values obtained from MDSC, DMA, and spectroscopic ellipsometry for the **PS** control are similar, falling within 10 °C of each other. However, for VAPNB **P2** and **P6**, a larger discrepancy (>30 °C) was observed. Similar results were found for the **P2P6** copolymer series (range of 30-50 °C). Each method showed a similar trend in that increasing the molar ratio of **M6** comonomer depressed the T_g, which was expected due to the increased flexibility of the ether linkage in monomer **M6** as compared to alkyl-substituted **M2**. With the exception of entry 3, T_g measurements obtained by MDSC and ellipsometry agree within 15 °C. This is consistent with a prior report that describes thermal characterization of VAPNB homopolymers,[33] and that can be attributed to the fact that

Table 2. T_g values of **PS**, **P2**, **P6**, and the **P2P6** copolymer series as measured by MDSC, DMA, and ellipsometry.

entry	polymer	T_g by MDSC (°C)	T_g by DMA (tan δ, °C)	T_g by ellipsometry (°C)[a]
1	**PS**	95[b]	104	100
2	**P2**	189	209	173
3	**P2^{86}P6^{14}**	186	202	154
4	**P2^{65}P6^{35}**	162	191	160
5	**P2^{28}P6^{72}**	163	191	160
6	**P6**	162	184	152

[a]Initial film thickness (h) was ~500 nm. [b]The T_g of PS was measured using conventional DSC.

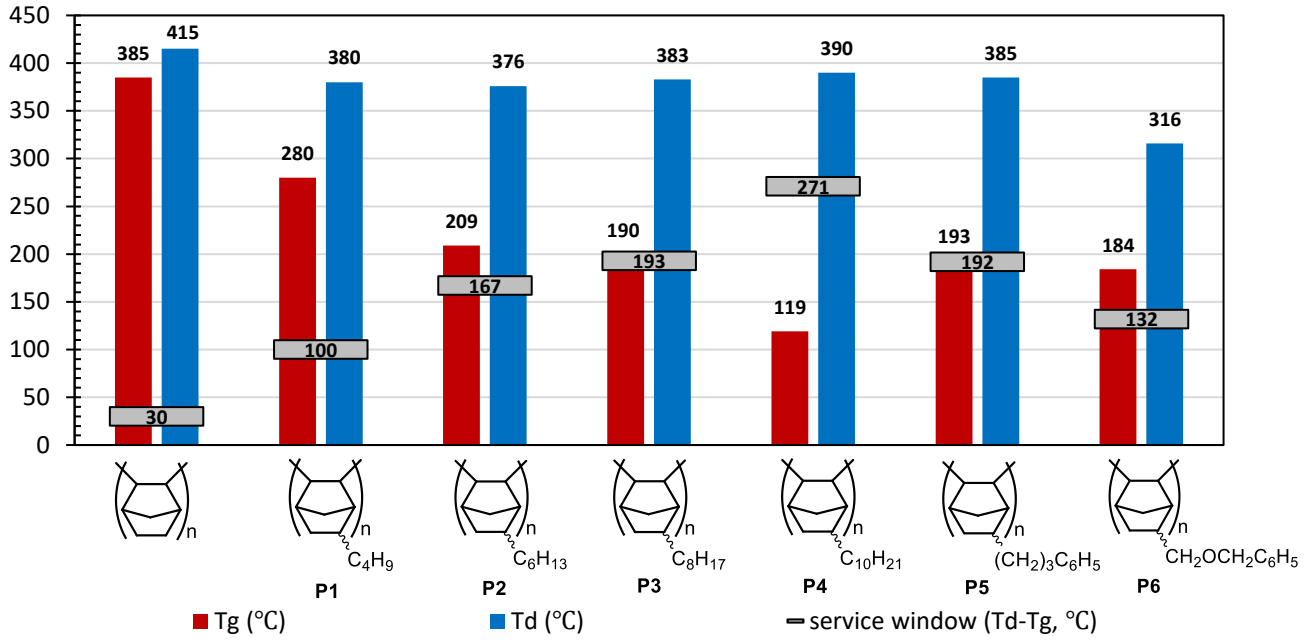

Figure 2. T_g, T_d, and service window (T_d-T_g) of unsubstituted VAPNB[3, 32] and substituted homo-VAPNBs **P1-P6**.

heat capacity and thermal expansion coefficient are both thermodynamic properties. The discrepancy between these methods and DMA is likely explained by the fact that DMA does not probe a thermodynamic property, but rather employs both mechanical and thermal stimulation to measure a viscoelastic response. Ultimately, DMA was selected as the most useful method for characterizing the T_g of the functionalized VAPNBs for a variety of reasons. First, the transitions obtained using MDSC and ellipsometry are extremely weak, and therefore difficult to detect and quantify with great accuracy (see Supporting Information, Figures S46-51). In contrast, the tan δ peak obtained via DMA is strong and readily identifiable. Second, viscoelastic response is arguably more relevant to the design and tailoring of melt-processable polymers. Finally, the T_g values obtained by DMA provide the most conservative estimate of the service window between T_g and T_d.

The T_g (via DMA), T_d, and service window of all the substituted VAPNB homopolymers are summarized in Figure 2 and Table S1. The T_g and T_d of unfunctionalized VAPNB are reported as approximately 390 °C and 415 °C, respectively.[3, 32] The T_gs of VAPNB homopolymers are significantly depressed by functionalization, which was expected due to the incorporation of flexible substituents.[49] Within the linear alkyl substituent series (**P1**-**P4**), the longer and more flexible substituents resulted in lower T_g's than their shorter analogues, with T_g decreasing from 280 °C for the butyl-substituted VAPNB (**P1**) to 119 °C for the decyl-substituted VAPNB (**P4**) (Figure 2). As shown in Figure S75, WAXS measurements of **P3** and **P4** do not detect any crystallization of the long alkyl substituents. The addition of rigid and bulky phenyl substituents into polymer **P5** introduces potential π-π stacking interactions (**P5**) and was expected to increase the T_g relative to an alkyl substituent with the same number of carbons. Indeed, the T_g of **P5** which contains nine carbon atoms in its sidechain is similar to that of **P3**, which contains only 8 carbon atoms (Figure 2). Furthermore, when ether linkages are introduced (**P6**), substituent flexibility is increased due to the lower rotational barrier of ethereal linkages as compared to analogous hydrocarbon linkers. This added flexibility results in T_g being depressed from 193 °C for phenylpropyl-substituted **P5** to 184 °C for benzyloxymethyl-substituted **P6**, despite having substituents of similar size and composition.

It should be noted that the T_gs of the VAPNBs synthesized herein are generally lower than previously reported in the literature. Examples include **P1** (280 °C) which has been previously reported to be 330 °C;[26] **P2** (209 °C) which has been previously reported to be 265 °C,[3] 280 °C,[13] or 225 °C;[26] and lastly, **P4** (119 °C) which has been previously reported to be 150 °C,[13] or 180 °C.[26] As discussed previously, we hypothesize that this difference in measured T_g values may be attributed to the different catalysts and/or the characterization method being employed.

The T_d's of VAPNB homopolymers are moderately depressed by functionalization, but aside from **P6**, all T_d's exceeded ~380 °C. By inspecting the TGA data, the degradation behavior of **P6** is different from **P1**-**P5**. Specifically, the derivative of the TGA curve of **P6** suggests there are two stages of degradation, the first of which we hypothesize is degradation of the ether linkage prior to the second stage of backbone degradation (see Supporting Information Figure S36). The key conclusion from the data in Figure 2 and Table S1 is that functionalization more strongly depresses T_g than T_d, leading to a large service window for melt processing, while T_g remains high enough to expect good thermomechanical stability. Furthermore, the T_g's and service windows of these VAPNB materials are comparable to those of commercial amorphous engineering thermoplastics, such as polycarbonate, and polyetherimide.[18, 22, 50]

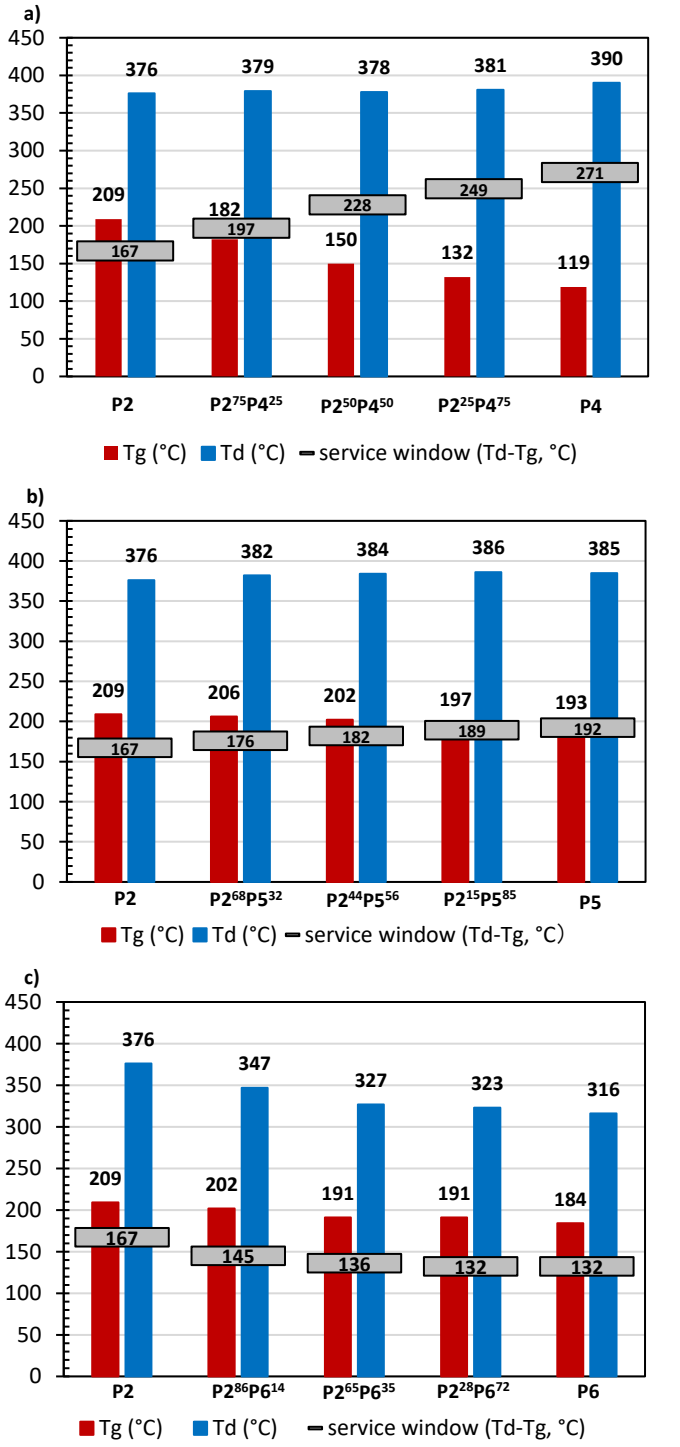

Figure 3. T_g, T_d, and service window for the a) **P2P4**, b) **P2P5**, and c) **P2P6** copolymer series.

We also envisioned that the thermal properties of these VAPNB materials may be tuned via copolymerization, rather than relying solely on a single substituent chemistry. As an example, the T_d's of **P2** and **P4** are both approximately 380 °C, yet the T_g's of **P2** and **P4** are 209 °C and 120 °C, respectively. This suggests that copolymerization of **M2** and **M4** may enable tailoring of VAPNB T_g across a broad 90 °C window with little impact on T_d. As shown in Figure 3 and Table S1, the T_g's of the **P2P4** copolymer series fall within the anticipated range and provide potential melt processing temperature ranging from 150-350 °C. Similarly, the **P2P5** and **P2P6** copolymer series also demonstrates that T_g's can be designed to fall in between their homopolymer analogues, though admittedly this range is small due to the small difference in T_g values for homopolymers **P2**, **P5**, and **P6**. Aside from the **P2P4** copolymer series that has high **M4** comonomer content, the T_g's of these statistical copolymers fall within the range of 180-280 °C. Furthermore, the measured T_d values for all copolymers exceeded ~380 °C, except the **P2P6** copolymer series which bears the **M6** ether-containing monomer units (Figures S43-45). The service windows of these copolymers are comparable to those of commercial amorphous engineering thermoplastics as well.

To better understand the relationship between copolymer T_g, comonomer composition, and potential intermolecular interactions present, we sought to compare our experimentally determined values to simple mathematical correlations. Starting with the alkyl substituted VAPNB copolymer series **P2P4**, theoretical copolymer T_g's were calculated using the Fox equation and compared to experimental T_g data obtained via DMA (Figure 4a). The Fox equation is as follows:

$$\frac{1}{T_g} = \frac{w_1}{T_{g1}} + \frac{1 - w_1}{T_{g2}}$$

where the parameters T_g, w_1, T_{g1}, and T_{g2} are the predicted glass transition temperature for the copolymer, the weight fraction of monomer type 1, and the measured glass transition temperatures of homopolymer types 1 and 2, respectively. The Fox equation provides excellent agreement with experimental data, confirming the validity of this simple model for alkyl substituted VAPNBs. Furthermore, there are no free parameters in this model, as T_{g1} and T_{g2} are measured from DMA. As a result, the T_g and service window can be predicted as a function of w_1 based solely on knowledge of the homopolymer T_g's.

In contrast to the simple alkyl substituted copolymer series **P2P4**, the **P2P5** series mixes hexyl and phenylpropyl substituents, where the latter substituent has bulkier side chains that have the potential to introduce π-π stacking interactions. As a result, chain packing in the solid state may be perturbed and experimental T_g values may be observed that deviate from those predicted using the simple Fox equation. As shown in Figure 4b, the **P2P5** copolymer series exhibits experimental T_g values that are larger than predicted using the simple Fox equation.

The **P2P6** series combines hexyl and benzyloxymethyl substituents, where the latter introduces a rigid and bulky pendant group, increased linkage flexibility, the potential for π-π stacking, and dipole-dipole interactions. As shown in Figure 4c, this series displays negative deviations from the Fox equation. To better estimate the copolymer thermal properties, the Gordon-Taylor equation is used to capture deviations from ideal behavior:[51, 52]

$$T_g = \frac{w_1 T_{g1} + k(1 - w_1) T_{g2}}{w_1 + k(1 - w_1)}$$

The variable k is an adjustable fitting parameter. For **P2P5** copolymer series, the trend is well-described with $k = 0.5$ (Figure 4b). Similarly, for **P2P6** copolymer series, an optimized value of k = 2.6 provides qualitative agreement with the experimental trends (Figure 4c).

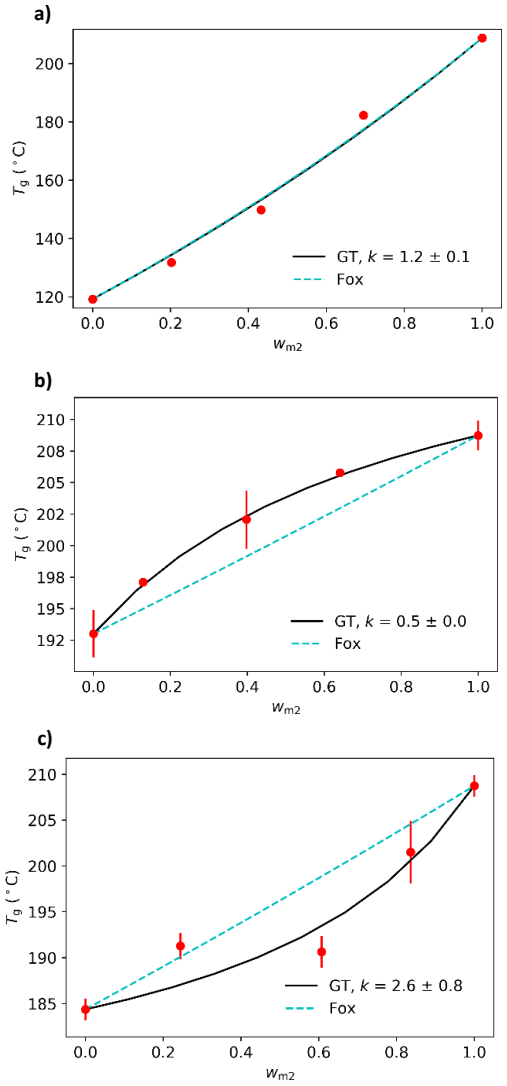

Figure 4. Comparison of experimental T_g (as determined by DMA) and theoretical T_g as predicted by the Fox and Gordon-Taylor equations for the a) **P2P4** series, b) **P2P5** series, and c) **P2P6** series. W_{m2} is defined in each plot as the weight fraction of comonomer **M2** in each copolymer. Error bars encompass the minimum and maximum values of two independent measurements. *Note:* in some series, the error bars are smaller than the symbol size.

While a broad service window is a requirement for melt processing, this criterion alone does not establish the suitability of a material for melt extrusion or injection molding. To demonstrate that substituted VAPNBs are indeed melt processable, homopolymer **P2** was selected as a model and compared to commercially available **PS**. As a note, the entanglement molecular weight (M_e) of **P2** is estimated to be 33.1 kg/mol,[53] and thus the samples synthesized herein (M_n = 163 kg/mol) are presumably entangled. As shown in Figure 5, polymer **P2** (T_g = 209 °C, T_d = 377 °C) was readily melt processed into bars at 250 °C under a nitrogen atmosphere. The microcompounder in which the melt was formed (for subsequent injection molding) had a force plateau after 10 min of processing, which was used to compare relative melt viscosity of PS and **P2** at low shear rate (90 rpm). In earlier work by Stretz and coworkers,[54] a **PS** (Styron 678 CW) sample reached 689 N of force when processed at 220 °C and 100 rpm; however, the commercial **PS** used in this study reached a force plateau of 1395 (± 12) N (5 replicates) at 210 °C and 90 rpm. This is remarkably similar to VAPNB **P2**, which reached a force plateau of 1483 (± 32) N (3 replicates) at 250 °C and 90 rpm. This comparison shows that **P2** may be readily processed in similarity to some **PS** samples, needing only slightly elevated melt temperatures (250 °C) that are close to the commercial processing temperatures of many other engineering polymers (e.g., nylon and polycarbonate).

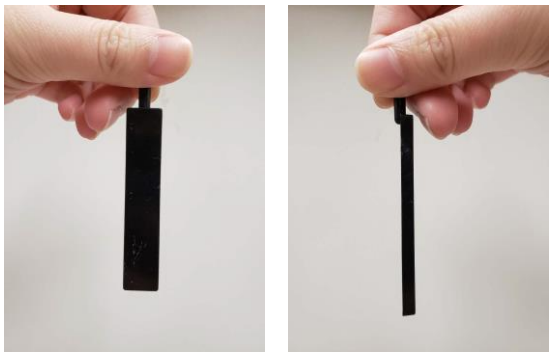

Figure 5. Melt extruded bars of VAPNB **P2**. The dark color is presumed to be a consequence of residual catalyst decomposition/oxidation that occurs during melt processing.

Three additional qualitative processing observations were noted during melt extrusion. First, the extrudate was quite elastic, retracting a bit when cut. Second, the volume of the compounder (controlled by overflow at manufacturer specification of 5 cm³) was constant, and the average masses of **PS** and **P2** melts were 2.43 g and 1.01 g, respectively. While these masses were recorded at different temperatures, the difference is larger than could be accounted for by temperature alone, suggesting that the **P2** melt is a low-density material. This may be one possible reason for **P2**'s surprisingly high degree of processibility compared to what might be expected for a rigid backbone polymer. Lastly, it was noted that the extruded specimens were dark in color, despite **P2** being colorless prior to processing. We hypothesize that this color results due to residual catalyst decomposition and/or oxidation during processing.[55] As a note, prior studies have shown that residual catalyst can be removed via a variety of methods, though this was not performed in this study.[14, 30, 55]

The mechanical properties of the melt processed, **P2** bar specimens were then evaluated via tensile testing. As shown in Figure 6, **P2** is softer (Young's modulus of 1291 MPa vs. 5765 MPa) and less brittle (0.01 mm/mm vs. 0.0025 mm/mm strain at yield) than **PS**. A cyclic loading test was also performed with **P2**, where the cyclic loading modulus is calculated to be 1349 MPa (Figure S72). While a complete study of substituted VAPNB mechanical properties is beyond the scope of this paper, these data demonstrate that melt processed VAPNBs have potential for real-world applications.

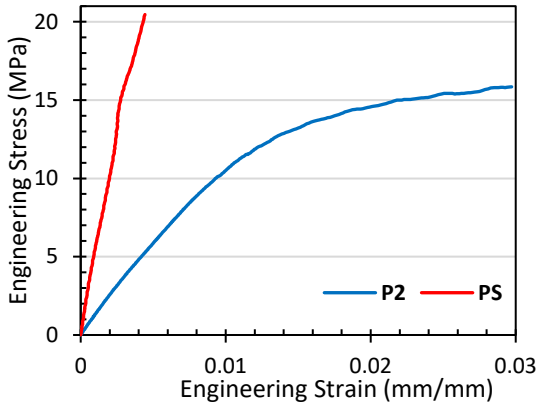

Figure 6. Stress-strain curves for polymers **P2** and **PS**.

To determine the intactness of the processed polymer **P2** after melt extrusion, thorough characterization of **P2** was performed before and after extrusion, including NMR, GPC, and DMA (see Supporting Information S68-S71). ^{1}H NMR spectroscopy revealed that a minor set of new peaks (~5.3 ppm, Figure S68) were present in the processed material that were not present prior to melting. We hypothesize that these resonances may result due to ring-opening of the bicyclic ring of VAPNB (around 3% of total, calculated by relative integration) to produce alkene containing polymers analogous to those of polynorbornene synthesized via ring-opening metathesis polymerization. This is supported by a recent report by Boydston and coworkers that demonstrates that many VAPNBs have intrinsic mechanochemical reactivity, producing partially ring-opened sequences along the main chain of VAPNBs when they are placed under mechanical activation (e.g. sonication).[56] We suspect that melt extrusion may act as a source of mechanical activation and lead to this conversion.

GPC characterization of melt processed **P2** revealed that molecular weight decreased from M_n = 163 to 117 kg/mol following melt extrusion and exhibited a slightly increased dispersity ($Đ$ = 1.83 vs. 1.60 for the original unprocessed sample) (Figure S69). This is consistent with previous reports in which polyolefins, such as polypropylene and polyethylene, undergo thermo-oxidative and/or thermo-mechanical induced chain scission.[57] Additionally, **P2**'s average T_g (from DMA) before and after melt extrusion was 209 °C and 205 °C, respectively. Though this observation is within one standard deviation of experimental results, the decreased T_g value is consistent with ^{1}H NMR spectroscopic analysis showing potential generation of ring-opened sequences along the main chain (Figure S70). Overall, it is concluded that the majority of the VAPNB **P2** is intact after melt extrusion, but a small portion of the polymer may undergo chain scission due to oxidation and/or mechanical activation. DMA analysis also revealed that the extruded material's storage modulus (E') (at 100 °C) decreased slightly from E' = 0.49 GPa before melt extrusion to E' = 0.32 GPa after melt extrusion. In contrast, loss modulus (E'') before and after melt extrusion were similar at 0.031 GPa and 0.027 GPa, respectively (Figure S71).

Conclusions

High molecular weight VAPNB homopolymers and copolymers bearing alkyl, aryl, and aryl ether functional groups were synthesized using a (η^3 - allyl)Pd(i-Pr$_3$P)Cl/ LiBAr$^F{}_4$ catalyst system. Each polymer's thermal characteristics (T_g, T_d, and service window T_d - T_g) were evaluated using DMA and TGA. The T_g of all synthesized homopolymers and copolymers were depressed relative to that of unfunctionalized VAPNB (ca. 385 °C). The extent of T_g depression was tuned by the chemical structure of the substituent and was found to follow anticipated trends with substituent size, flexibility, and types of molecular interactions. Notably, the T_g remained at or above 150 °C for most samples, an important attribute for engineering thermoplastics. The T_d of VAPNBs with alkyl and aryl substituents was approximately 380 °C, which is slightly depressed relative to unfunctionalized VAPNB (ca. 415 °C), In contrast, the T_d of VAPNBs with ethereal substituents ranged from approximately 320-340 °C.

A key outcome of these studies is that VAPNB substituents have a much larger effect on T_g than T_d, so it is possible to broaden the service window from approximately 30 °C for unsubstituted VAPNB to 200 °C, all while maintaining a sufficiently high T_g to maintain mechanical integrity. To further establish the viability of melt processing, a functionalized VAPNB with T_g of 209 °C and T_d of 377 °C was melt extruded and molded into bars at 250 °C. The bars were subjected to tensile and DMA tests and then dissolved for characterization by GPC and NMR. These post-extrusion analyses demonstrate that melt processed VAPNBs show only minor signs of degradation from processing at high temperatures under flow.

Conflicts of interest

There are no conflicts to declare.

Acknowledgements

This work is supported in part by the American Chemical Society Petroleum Research Fund (ACS-PRF, Award # 59132-ND7), and in part by the U.S. Department of Energy's Office of Energy Efficiency and Renewable Energy (EERE) under the award number DE-EE0009177 provided to the University of Tennessee – Oak Ridge Innovation Institute (UT-ORII). XW was supported in part by the ACS-PRF and the UT-ORII Science Alliance Graduate Advancement, Training, and Education (GATE) program. A portion of the research was conducted at the Center for Nanophase Materials Sciences (CNMS), which is a DOE Office of Science User Facility. The authors thank Yangyang Wang (Oak Ridge National Laboratory, CNMS) for assistance with DMA and MDSC experiments. WAXS experiments were enabled by the Major Research Instrumentation program of the National Science Foundation under Award No. DMR-1827474. The authors also thank Boulder Scientific for their generous donation of LiBAr$^F{}_4$.

Note and References

‡ Tabulated thermal data; NMR spectra of monomer and polymers; GPC plots of polymers; TGA, DSC, spectroscopic ellipsometry, DMA traces; catalyst effect on polymer thermal properties; data comparing **P2** before and after melt extrusion; and molecular weight influence on polymer thermal properties can be found in the Supporting information.

1. E. S. Finkelshtein, M. V. Bermeshev, M. L. Gringolts, L. Starannikova and Y. P. Yampolskii, *Russ. Chem. Rev.*, 2011, **80**, 341.
2. K. H. Park, R. J. Twieg, R. Ravikiran, L. F. Rhodes, R. A. Shick, D. Yankelevich and A. Knoesen, *Macromolecules*, 2004, **37**, 5163-5178.
3. N. R. Grove, P. A. Kohl, S. A. Bidstrup Allen, S. Jayaraman and R. Shick, *J. Polym. Sci. B Polym. Phys.*, 1999, **37**, 3003-3010.
4. M. Chen, W. Zou, Z. Cai and C. Chen, *Polym. Chem.*, 2015, **6**, 2669-2676.
5. Y. Bai, P. Chiniwalla, E. Elce, R. A. Shick, J. Sperk, S. A. B. Allen and P. A. Kohl, *J. Appl. Polym. Sci.*, 2004, **91**, 3023-3030.
6. *WO Pat.,* 95/14048, 1995.
7. B.-G. Shin, T.-Y. Cho, D. Y. Yoon and B. Liu, *Macromol. Res.*, 2007, **15**, 185-190.
8. S. Breunig and W. Risse, *Die Makromolekulare Chemie: Macromol. Chem. Phys.*, 1992, **193**, 2915-2927.
9. W. Zhou, X. He, Y. Chen, M. Chen, L. Shi and Q. Wu, *J. Appl. Polym. Sci.*, 2011, **120**, 2008-2016.
10. K. R. Gmernicki, E. Hong, C. R. Maroon, S. M. Mahurin, A. P. Sokolov, T. Saito and B. K. Long, *ACS Macro Lett.*, 2016, **5**, 879-883.
11. D.-G. Kim, T. Takigawa, T. Kashino, O. Burtovyy, A. Bell and R. A. Register, *Chem. Mater.*, 2015, **27**, 6791-6801.
12. S. V. Mulpuri, J. Shin, B.-G. Shin, A. Greiner and D. Y. Yoon, *Polymer*, 2011, **52**, 4377-4386.
13. K. D. Dorkenoo, P. H. Pfromm and M. E. Rezac, *J. Polym. Sci. B Polym. Phys.*, 1998, **36**, 797-803.
14. E. C. Kim, M.-J. Kim, L. N. Thi Ho, W. Lee, J.-W. Ka, D.-G. Kim, T. J. Shin, K. M. Huh, S. Park and Y. S. Kim, *Macromolecules*, 2021, DOI: 10.1021/acs.macromol.1c00858.
15. C. R. Maroon, J. Townsend, K. R. Gmernicki, D. J. Harrigan, B. J. Sundell, J. A. Lawrence III, S. M. Mahurin, K. D. Vogiatzis and B. K. Long, *Macromolecules*, 2019, **52**, 1589-1600.
16. S. Liu, Y. Chen, X. He, L. Chen and W. Zhou, *J. Appl. Polym. Sci.*, 2011, **121**, 1166-1175.
17. M. Mandal, G. Huang and P. A. Kohl, *J. Membr. Sci.*, 2019, **570**, 394-402.
18. A. C. Kuo, *Polymer data handbook*, Oxford University Press, Inc, 1999.
19. E. J. Stober and J. C. Seferis, *Polym. Eng. Sci.*, 1988, **28**, 634-639.
20. G. Molnár, A. Botvay, L. Pöppl, K. Torkos, J. Borossay, Á. Máthé and T. Török, *Polym. Degrad. Stab.*, 2005, **89**, 410-417.
21. G. Lisa, E. Avram, G. Paduraru, M. Irimia, N. Hurduc and N. Aelenei, *Polym. Degrad. Stab.*, 2003, **82**, 73-79.
22. L. Perng, *J. Appl. Polym. Sci.*, 2001, **79**, 1151-1161.
23. A. S. Alaboodi and S. Sivasankaran, *J. Manuf. Process*, 2018, **35**, 479-491.
24. *US Pat.,* 20210198392, 2021.
25. B. L. Goodall, in *Late transition metal polymerization catalysis*, ed. L. S. B. Bernhard Rieger, Smita Kacker, Susanne Striegler, WILEY-VCH Verlag GmbH & Co. KGaA, Weinheim, 2003, ch. 4, pp. 101-154.
26. W. McDougall, S. Farling, R. Shick, S. Glukh, S. Jayaraman, L. Rhodes, R. Vicari, P. Kohl, S. Bidstrup-Allen and P. Chiniwalla, *Avatrel™ dielectric polymers for HDP applications*, Proc. International Conference and Exhibition on High-Density Interconnect and Systems Packaging, Denver, CO, USA, 1999.
27. B. Goodall and D. Barnes, *Polym. Prepr. (Am. Chem. Soc., Div. Polym. Chem.)*, 1998, **39**, 216-217.
28. *US Pat.,* 5468819, 1995.
29. *US Pat.,* 5705503, 1998.
30. D.-G. Kim, A. Bell and R. A. Register, *ACS Macro Lett.*, 2015, **4**, 327-330.
31. S. D. Tsai and R. A. Register, *Macromol. Chem. Phys.*, 2018, **219**, 1800059.
32. A. S. Abu-Surrah, U. Thewalt and B. Rieger, *J. Organomet. Chem.*, 1999, **587**, 58-66.
33. E. A. Lewis and B. D. Vogt, *J. Polym. Sci. B Polym. Phys.*, 2018, **56**, 53-61.
34. J. Lipian, R. A. Mimna, J. C. Fondran, D. Yandulov, R. A. Shick, B. L. Goodall, L. F. Rhodes and J. C. Huffman, *Macromolecules*, 2002, **35**, 8969-8977.
35. P. Leber, K. Kidder, D. Viray, E. Dietrich‐Peterson, Y. Fang and A. Davis, *J. Phys. Org. Chem.*, 2018, **31**, e3888.
36. H. Koch and W. Haaf, *Justus Liebigs Ann. Chem.*, 1960, **638**, 111-121.
37. M. Jean and P. Van de Weghe, *Tetrahedron Lett.*, 2011, **52**, 3509-3513.
38. J. M. Blanco, F. Fernández, X. García-Mera and J. E. Rodríguez-Borges, *Tetrahedron*, 2002, **58**, 8843-8849.
39. S. H. Kim, M. A. Worsley, C. A. Valdez, S. J. Shin, C. Dawedeit, T. Braun, T. F. Baumann, S. A. Letts, S. O. Kucheyev and K. J. J. Wu, *RSC Adv.*, 2012, **2**, 8672-8680.
40. T. G. Driver, A. K. Franz and K. Woerpel, *J. Am. Chem. Soc.*, 2002, **124**, 6524-6525.
41. K. Müller, S.-H. Chun, A. Greiner and S. Agarwal, *Des. Monomers Polym.*, 2005, **8**, 237-248.
42. A. Richard, *Faraday Discuss.*, 1994, **98**, 219-230.
43. D. A. Barnes, G. M. Benedikt, B. L. Goodall, S. S. Huang, H. A. Kalamarides, S. Lenhard, L. H. McIntosh, K. T. Selvy, R. A. Shick and L. F. Rhodes, *Macromolecules*, 2003, **36**, 2623-2632.
44. D. A. Alentiev, M. V. Bermeshev, L. E. Starannikova, E. V. Bermesheva, V. P. Shantarovich, V. G. Bekeshev, Y. P. Yampolskii and E. S. Finkelshtein, *J. Polym. Sci. A Polym. Chem.*, 2018, **56**, 1234-1248.
45. R. García‐Loma and A. C. Albéniz, *Asian J. Org. Chem.*, 2019, **8**, 304-315.
46. A. D. Hennis, J. D. Polley, G. S. Long, A. Sen, D. Yandulov, J. Lipian, G. M. Benedikt, L. F. Rhodes and J. Huffman, *Organometallics*, 2001, **20**, 2802-2812.
47. S. Kim, S. Hewlett, C. Roth and J. M. Torkelson, *Eur. Phys. J. E. Soft Matter*, 2009, **30**, 83.
48. P. Gill, S. Sauerbrunn and M. Reading, *J. Therm. Anal.*, 1993, **40**, 931-939.
49. G. Odian, *Principles of polymerization*, John Wiley & Sons, 4th edn., 2004.

50. P. Patel, T. R. Hull, R. W. McCabe, D. Flath, J. Grasmeder and M. Percy, *Polym. Degrad. Stab.*, 2010, **95**, 709-718.
51. E. Penzel, J. Rieger and H. Schneider, *Polymer*, 1997, **38**, 325-337.
52. M. Gordon and J. S. Taylor, *J. Appl. Chem.*, 1952, **2**, 493-500.
53. K. Müller, S. Kreiling, K. Dehnicke, J. Allgaier, D. Richter, L. J. Fetters, Y. Jung, D. Y. Yoon and A. Greiner, *Macromol. Chem. Phys.*, 2006, **207**, 193-200.
54. H. Stretz and D. Paul, *Polymer*, 2006, **47**, 8527-8535.
55. *WO Pat.,* 2003050158A1, 2003.
56. D. C. Lee, V. K. Kensy, C. R. Maroon, B. K. Long and A. J. Boydston, *Angew. Chem.*, 2019, **131**, 5695-5698.
57. H. Hinsken, S. Moss, J.-R. Pauquet and H. Zweifel, *Polym. Degrad. Stab.*, 1991, **34**, 279-293.